Modeling MESFETs and HEMTs Intermodulation Distortion Behavior Using a Generalized Radial Basis Function Network

J. A. García,[1] A. Tazón Puente,[1] A. Mediavilla Sánchez,[1] I. Santamaría,[1] M. Lázaro,[1] C. J. Pantaleón,[1] J. C. Pedro[2]

[1]Departamento Ingeniería de Comunicaciones, Universidad de Cantabria, Avda. Los Castros s/n 39005 Santander, Spain; e-mail: jangel@dicom.unican.es
[2]Instituto de Telecomunicações, Universidade de Aveiro, 3810 Aveiro, Portugal

ABSTRACT: This paper proposes a generalized radial basis function (GRBF) network to accurately describe drain to source current nonlinearity for intermodulation distortion (IMD) prediction of MESFETs and HEMTs applications in their saturated region. Trying to analytically reproduce the nonlinearities second and third order Taylor-series coefficients, responsible for IMD performance in these devices, may result in a quite difficult task. Neural networks were introduced as a robust alternative for microwave modeling, mostly employing the black-box model type approach of the multilayer perceptron network. The GRBF network we consider is a generalization of the RBF network, which takes advantage of problem dependent information. Allowing different variances for each dimension of input space, the GRBF network makes use of soft nonlinear dependence of the drain to source current derivatives with drain to source voltage for improving accuracy at reduced cost. The network structure and its learning algorithm are presented. Results of its performance are compared to other structures with similar amounts of parameters. Carrier to intermodulation (C/I) predictions validate this approach for precise IMD control versus bias and load in class A amplifiers applications. © 1999 John Wiley & Sons, Inc. Int J RF and Microwave CAE 9: 261–276, 1999.

Keywords: MESFETs; HEMTs; neural networks; modeling; intermodulation distortion

I. INTRODUCTION

Predicting nonlinear distortion phenomena results is of great concern for the microwave community nowadays. The emerging multiple-carrier communication systems have been determining important efforts in analysis techniques and accurate modeling at device, circuit, and system levels.

MESFETs and HEMTs constitute the most widely employed transistors in microwave and millimeter wave applications, thus concentrating the modeling activities for some years [1, 2]. However, most of these venerable models were not conceived for intermodulation distortion (IMD) prediction and have poor performance when this nonlinear behavior either in large-signal or small-signal regimes is of primary interest.

Reproducing the small-signal third order IMD on a nonlinear device is quite a difficult and common task (amplifiers working below the 1 dB compression point and mixers excited by small RF signals when compared to the local oscillator are typical examples). Having success is only possible if its model not only describes the nonlinear current–voltage (I/V) and charge–voltage (Q/V) characteristics, but also their respective derivatives up to the same order [3]. Successive numeric differentiations or least squares fittings of the commonly measured characteristics for a mild nonlinear device (MESFETs and HEMTs are in-

Correspondence to: J. A. García.

CCC 1096-4290/99/030261-16

cluded) just exacerbate the measurement noise and hide the nonlinear properties these coefficients enclose.

Trying to accurately reproduce IMD in 50 Ω or similar conditions for applications in the saturated region first requires the experimental extraction of the transconductance coefficients from harmonic measurements [4]. A proper load control needs however, a two-sided description of the drain to source current Ids(Vgs, Vds) in the model of Figure 1 with a procedure like [5]. High frequency IMD contribution of the minor nonlinearity Cgs(Vgs) could be also included with a technique like the one we proposed in [6].

Standard modeling approaches employ analytical expressions for the nonlinearities in terms of the control voltages. Some simple functions could be appropriate if we are just interested in reproducing the absolute nonlinear characteristic, but this would not be the case when concerned in simultaneously adjusting the derivatives up to the third order in the particular operating region. Look-up table options [7] would also be difficult to generate and manage when we try to find a good trade-off between gain and C/I for a highly linear design controlling both biases (Vgso and Vdso) as well as the load condition.

On the other hand, neural networks have emerged as a robust tool at device level, here of our concern, for modeling microwave components such as microstrip vias [8], interconnects [8, 9], spiral inductors [10], coplanar waveguide elements [11], waveguide filters [12], and FETs [13–15]. They have been mainly employed as an effective way of substituting complex electromagnetic (EM)–physics calculations in optimization and statistical design. They have also been introduced for constructing a large-signal description from the small signal linear elements dependence with the bias voltages [16] and for IMD prediction from pulsed measurements [17], both with the empirical basis and the circuital description so widely employed by microwave designers. Important applications not at device but at circuit level, have also been reported [9, 13–15].

As usually happens in other fields, all of these neural approaches almost only consider the use of the multilayer perceptron (MLP) with its backpropagation training algorithm. As discussed in [15], MLP networks are black-box type models quite flexible for applications of different nature, but do not take advantage of the problem nature information. MLP may need large amounts of training data or hidden neurons, and consequently coefficients, to ensure model accuracy.

In this paper we make use of a generalized radial basis function (GRBF) network to model the coefficients of the Ids(Vgs, Vds) complete two-sided Taylor-series expansion in the saturated region for both a MESFET and a HEMT to be properly included in a Volterra type simulator for IMD calculations on a small-signal regime. The GRBF network generalizes the RBF network concept, allowing different variances for each dimension of the input space (two in our case for the bias voltages Vgso and Vdso). By replacing the typical radial Gaussian kernels of RBF networks with elliptical basis functions, we are able to take advantage of the soft nonlinear dependence of the network's outputs (the DC value and the nine first, second, and third order terms) with the drain to source bias voltage in this operating region. This could be thought of as a microwave knowledge incorporated to the network, resulting in a sort of knowledge-based neural model, a concept proposed and effectively employed in [15, 18].

This paper is organized as follows. Section II reviews some aspects of nonlinear FET characterization for IMD purposes. Section III describes the GRBF network and its associated training algorithm. Section IV compares model accuracy and cost in different neural network approaches for this particular problem. Section V finally presents experimental results and simulations of C/I ratio vs. gate bias and load condition to verify the robustness of this approach for IMD accurate control at device level.

II. NONLINEAR CHARACTERIZATION OF FET DEVICES FOR INTERMODULATION DISTORTION DESCRIPTION

There is a number of different tools for nonlinear microwave analysis, some of them as harmonic balance are preferred for large signal regime with few noncommensurate excitations, while others as spectral balance are adequate for strong nonlinear condition with multiple carriers. For a small-signal regime, the tool for excellence has been the Volterra-series analysis, and particularly the nonlinear currents technique [19, 20].

Volterra-series description or nonlinear transfer functions approach is based on a Taylor-series

expansion of the device nonlinearities around a fixed bias point for amplifiers type applications or around a time-varying large signal waveform for mixers.

The predominant nonlinearity in the FET nonlinear equivalent circuit of Figure 1 is the drain to source current Ids(Vgs, Vds). Its two-sided power-series expansion around the bias point could be written as

$$\begin{aligned} &\mathrm{Ids}(\mathrm{Vgs}, \mathrm{Vds}) \\ &\quad = \mathrm{Ids}(\mathrm{Vgso}, \mathrm{Vdso}) + \mathrm{Gm1}.\mathrm{vgs} + \mathrm{Gds}.\mathrm{vds} \\ &\qquad + \mathrm{Gm2}.\mathrm{vgs}^2 + \mathrm{Gmd}.\mathrm{vgs}.\mathrm{vds} \\ &\qquad + \mathrm{Gd2}.\mathrm{vds}^2 + \mathrm{Gm3}.\mathrm{vgs}^3 \\ &\qquad + \mathrm{Gm2d}.\mathrm{vgs}^2.\mathrm{vds} \\ &\qquad + \mathrm{Gmd2}.\mathrm{vgs}.\mathrm{vds}^2 + \mathrm{Gd3}.\mathrm{vds}^3, \end{aligned} \tag{1}$$

where Ids(Vgso, Vdso) represents the DC value at the internal bias voltages Vgso and Vdso. The uppercases Ids, Vgs, and Vds represent the total magnitudes and the lowercases their corresponding small-signal time-varying components. The Gs are the Taylor coefficients of first (Gm1 and Gds), second (Gm2, Gmd, and Gd2), and third order (Gm3, Gm2d, Gmd2, and Gd3), associated to the derivatives as in [5, 21].

In Figure 2, we show typical values of Gm1 and Gm3, related to the first and third derivatives of Ids with Vgs, vs. Vgso at a Vdso in the saturated region for a MESFET (NE72084) and a HEMT (DO2AH). The experimentally extracted values were obtained from *S* parameters using Dambrine technique [22] for the first order ones, say Gm1 and Gds, and following the procedure in [5] with a similar test set-up for the rest.

The transconductance Gm1 fundamentally determines the device output power behavior vs. Vgso as we can observe in Figure 3a for the MESFET. The real part of the load impedance (RL) only contributes for values up to the order of 1/Gds as it is expected for an approximate parallel combination of both elements (see Fig. 1).

The Gm3 behavior is predominant for the in-band third order distortion products, 2f1-f2 and 2f2-f1, in the case of the standard two tones IMD experiment in low load condition, as it is shown in Figure 3b. In the MESFET, we can point out the existence of one null of Gm3 in the region of high Gm1, related to the observed maximum in the C/I ratio; this bias point results of great interest for low distortion designs and it is rarely reproduced even in models that are continuous in their derivatives. Most of the widely employed models, that are discontinuous at pinch-off or have a polynomial dependence [1], behave even worse for small-signal IMD prediction.

We can observe, however, a displacement of this interesting optimum bias point with RL. This

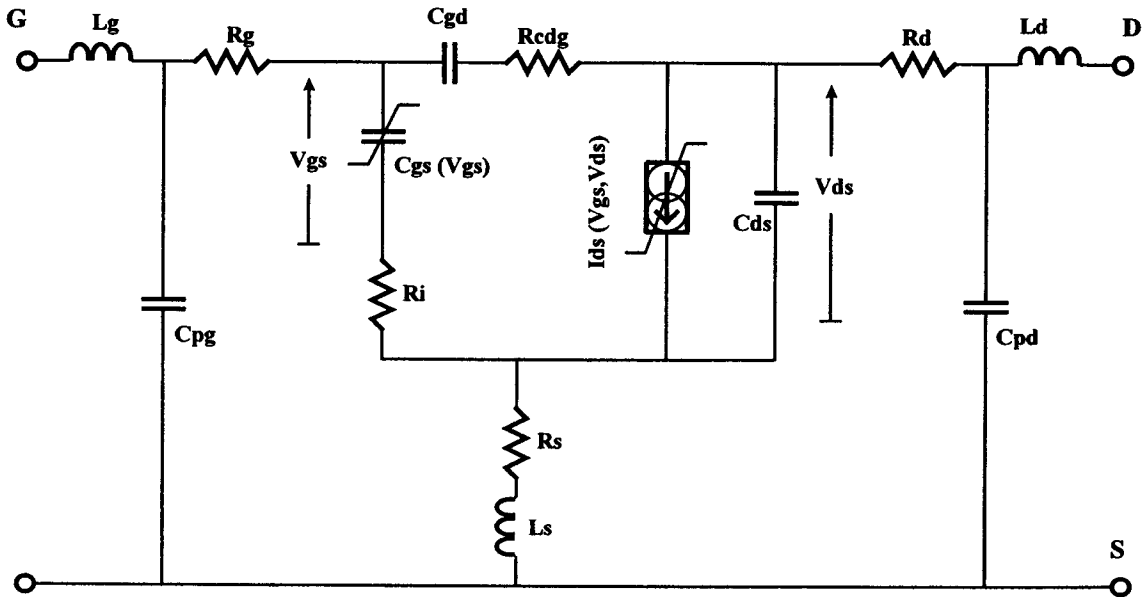

Figure 1. MESFET nonlinear equivalent circuit.

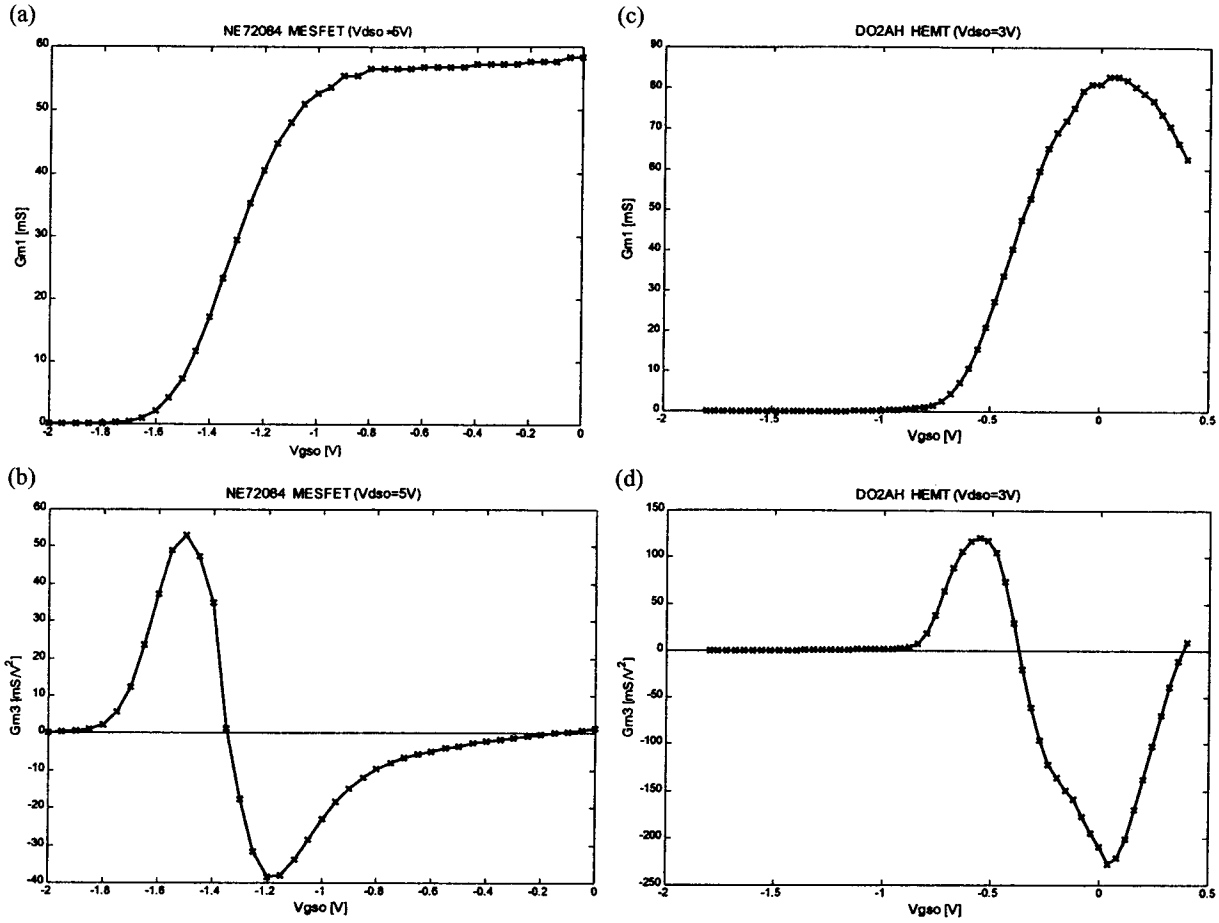

Figure 2. First and third order transconductance coefficients in the saturated region. (a) Gm1 and (b) Gm3 for a MESFET. (c) Gm1 and (d) Gm3 for a HEMT.

behavior is due to the rest of the third order coefficients (Gm2d, Gmd2 and Gd3) whose IMD contribution grows with RL. In [5] and [23] this cancellation of Gm3 contribution by the cross terms have been shown to be responsible for the existence of optimum load values for high C/I distortion ratio.

At low frequencies, if we consider the capacitors as opens and the inductors as shorts, we can approximate the vds/vgs ratio for a gate excitation as

$$\mathrm{Kv} = \frac{\mathrm{vds}}{\mathrm{vgs}} = -\frac{\mathrm{Gm1.(Rs + Rd + RL)}}{1 + \mathrm{Gds.(Rs + Rd + RL)}}. \quad (2)$$

When we vary RL, the magnitude of this term grows linearly for RL values up to the order of 1/Gds (it approaches Gm1/Gds for high RL). In this RL interval the contribution of Gm2d in (1) will grow linearly, with a quadratic law for Gmd2 and following a cubic one for Gd3. Thus:

$$\begin{aligned}&\mathrm{Ids(Vgs, Vds)}\\ &\quad = \cdots + (\mathrm{Gm3} + \mathrm{Gm2d.Kv}\\ &\qquad + \mathrm{Gmd2.Kv^2} + \mathrm{Gd3.Kv^3}).\mathrm{vgs^3} + \cdots .\end{aligned} \quad (3)$$

Taking into account the negative sign in Kv and the signs of the third order coefficients we can easily justify the cancellation phenomena. In both [5] and [23] the reader can find a detailed mathematical discussion.

Being able to predict the loadpull performance of C/I ratio is certainly a quite complex task, since we need not only to reproduce the predominant transconductance derivatives but also the referred cross and output coefficients.

If we want to accurately reproduce all the derivatives with an analytical function, we may be

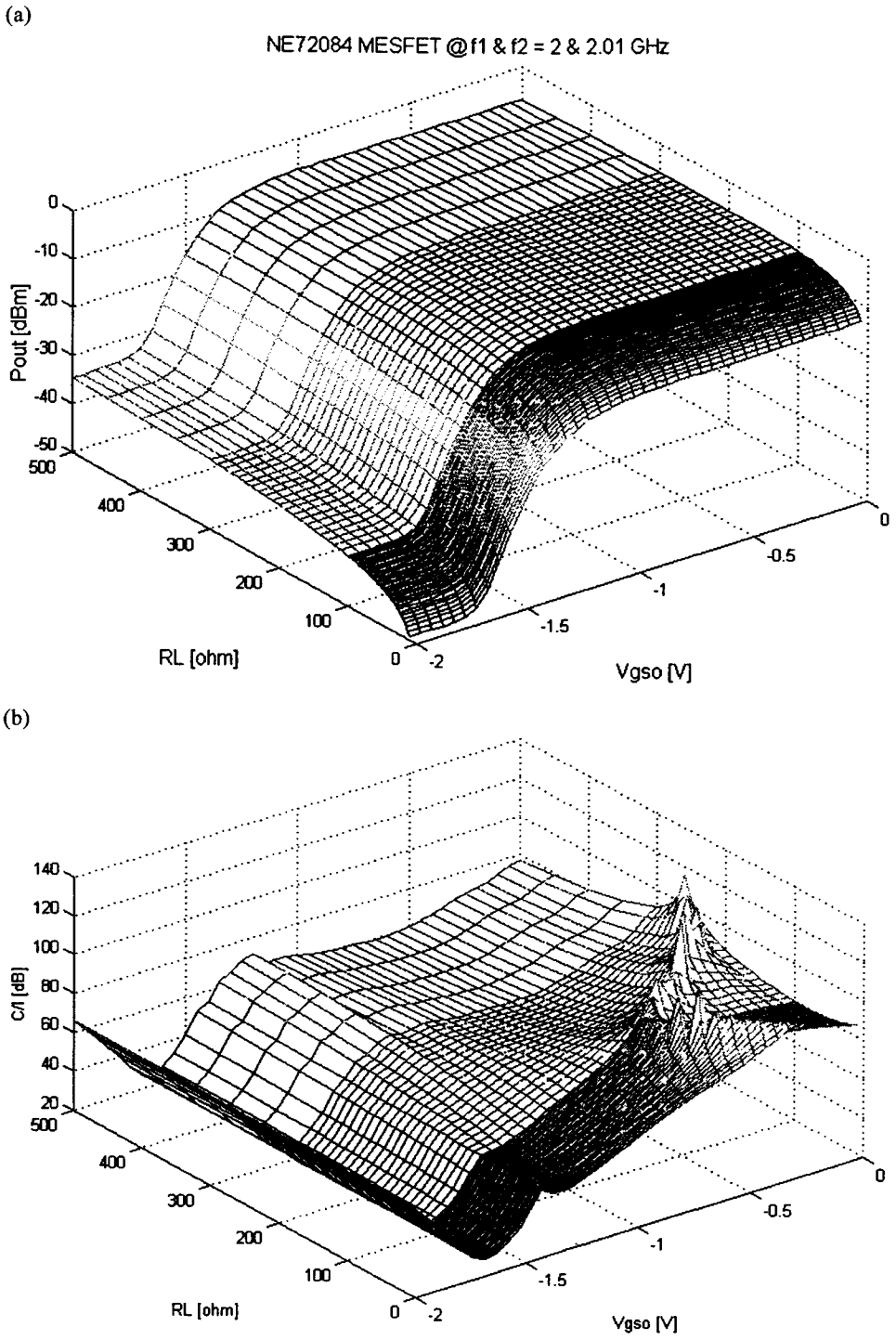

Figure 3. Pout (a) and C/I (b) behavior vs. bias and load for a NE72084 MESFET.

forced to employ an extremely complex formulation whose adjustment procedure could be critical. Look-up tables would also be difficult to manage for this case. Neural networks could however provide us with a robust solution. They were used in [17] to model Ids behavior from pulsed measurements in order to assure large-signal performance and to take advantage from neural networks' continuity for the derivatives reproduction. The derivatives were in fact continuous, but some

important differences appeared with the measured values since the derivatives information was not employed to construct the model, and pulsed measurements errors could perfectly hide higher order dependence in a mildly nonlinear device.

For an accurate IMD control at device level, we suggest a solution of the kind of [16] but with the coefficients of the Taylor-series expansion for Ids(Vgs, Vds) as outputs in the training set. In short, we are faced to the problem of obtaining a function (model) **G**: $R^2 \rightarrow R^{10}$ that approximates the nonlinear mapping from the input space of bias voltages **V** = (Vdso, Vgso), to the output space of model parameters **G(V)** = (Idso, Gm1, Gds, Gm2, Gmd, Gd2, Gm3, Gm2d, Gmd2, Gd3). Although the input space contains bias voltages, represented above with "o," we obviate it in the next section for notation simplicity when describing the network details.

III. GENERALIZED RADIAL BASIS FUNCTION NETWORK

A. Network Structure

The nonlinear input–output mapping between the bias voltages and the transistor model parameters could be described using universal approximators such as the radial basis function (RBF) or the multilayer perceptron (MLP) as feedforward layered networks. An RBF unit using a Gaussian kernel performs a local approximation, while an MLP constructs a global one to the input–output mapping. RBF networks result of larger size for input spaces of high dimension, but also of faster training due to the linear characteristic of their output layer.

Our model considers an extension of the RBF network which allows a different variance for each input dimension. The relaxation of the radial constraints transforms the standard Gaussian kernels with circular symmetry into elliptic basis kernels, which can reduce the dimensionality of the input space. This scheme is denoted as the generalized radial basis function (GRBF) network [24].

The hyperellipses around the centers of the basis functions were considered in [25] and a generalization of the elliptic kernel (Gaussian bar unit) was proposed in [26]. However, this generalization sums the weighted Gaussian responses along each input dimension, while the conventional RBF and the GRBF obtain a nonweighted product.

For notation simplicity, let us decompose the global mapping performed by the GRBF network (**G**: $R^J \rightarrow R^M$) into a set of single-output networks as follows:

$$\mathbf{G}(\mathbf{V}) = [g_1(\mathbf{V}), \ldots, g_M(\mathbf{V})], \tag{4}$$

each scalar output is given by

$$g_k(\mathbf{V}) = \sum_i \lambda_{ki} \sum_j e^{-(V_j - \mu_{ij})^2/2\cdot\sigma_{ij}^2} \rightarrow k = 1, \ldots, M, \tag{5}$$

where i is the index of the GRBF units, j the input dimensions, and k the outputs. In Figure 4

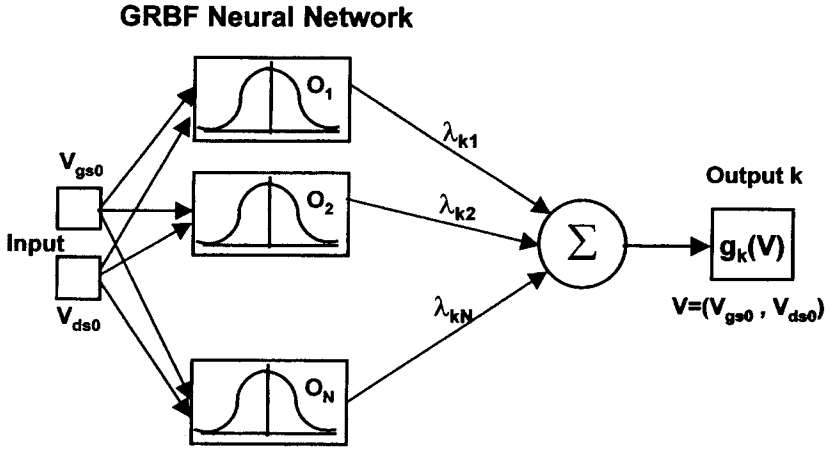

Figure 4. GRBF network structure for the kth output.

we show a diagram corresponding to one of these scalar outputs.

The GRBF can be viewed as an RBF where the Euclidean norm has been replaced by a weighted norm:

$$\|\mathbf{V} - \mu_i\|_{\mathbf{W}}^2 = (\mathbf{V} - \mu_i)^T \cdot \mathbf{W}^T \cdot \mathbf{W} \cdot (\mathbf{V} - \mu_i), \quad (6)$$

where $\mathbf{W}$ is a square matrix and T indicates the transpose. In this paper we consider a simplified version of the GRBF network which uses a diagonal weighting matrix $\mathbf{W}$ [Eq. (5)], we allow the variances to vary along each input dimension, but we do not allow the elliptic kernels to rotate.

To understand the application of a GRBF network to the MESFET intermodulation problem, we can observe Figure 5b and c. It shows the measured coefficients Gm2 (second order) and Gm3 (third order) as a function of the bias point $\mathbf{V} = (\text{Vgso}, \text{Vdso})$. As we can see, the shape of these coefficients along the Vgso axis could be approximated by a combination of Gaussians or even by a single one as in the case of Gm2; however, they have a quasilinear dependence with Vdso.

In order to adjust a neural model with a minimum number of parameters, we can take advantage of the nature of the problem following previous ideas [15, 18]. If the activation functions in the hidden layer were able to respond to a localized region along Vgso and to a nonlocalized region along Vdso; the soft nonlinear dependence of the drain to source current with one of the control voltages (Vdso), could be included as a knowledge in the network.

The GRBF network is not only capable of attaining this semilocal behavior, by allowing a different variance for each input dimension; but it is also appropriate to approximate, by broadening the variance along both directions, some parameters of the model that do not have a Gaussian shape along Vgso. This is the case of the MESFET first order Gm1 and Gds (see Fig. 5a).

B. Network Training

For the GRBF networks, some modifications of the learning strategy, as employed in RBF networks, are required in order to obtain an efficient model. First, the variances along each direction and the centers are obtained by applying a gradient descent algorithm. The gradient equations are given by

$$\frac{\partial E}{\partial \sigma_{ij}} = -2 \cdot \sum_p \sum_k e_k(\mathbf{V}_p) \cdot o_i(\mathbf{V}_p) \cdot \lambda_{ik} \cdot \frac{1}{\sigma_{ij}} \cdot \left(\frac{V_{pj} - \mu_{ij}}{\sigma_{ij}} \right)^2, \quad (7)$$

$$\frac{\partial E}{\partial \mu_{ij}} = -2 \cdot \sum_p \sum_k e_k(\mathbf{V}_p) \cdot o_i(\mathbf{V}_p) \cdot \lambda_{ik} \cdot \frac{1}{\sigma_{ij}} \cdot \left(\frac{V_{pj} - \mu_{ij}}{\sigma_{ij}} \right), \quad (8)$$

where p indexes the input patterns and k the output dimensions, $e_k(\mathbf{V}_p) = y_k(\mathbf{V}_p) - g_k(\mathbf{V}_p)$ is the network error for the kth output component, and

$$o_i(\mathbf{V}_p) = \prod_j e^{-(V_{pj} - \mu_{ij})^2 / 2 \cdot \sigma_{ij}^2} \quad (9)$$

is the output of the ith unit.

The second modification consists of selecting the GRBF units one by one until the squared error decreases below some threshold or a maximum number of units is reached. Looking again at Figure 5b we can understand the benefits of the proposed procedure: the Gm2 parameter can be approximated by placing a single GRBF unit and broadening its variance σ_{ij} along the drain to the source input voltage direction. Therefore, the selection of the GRBF units one by one let us take full advantage of their semilocal approximation capabilities.

The algorithm employed to model Ids derivatives behavior can be summarized in the following steps:

1. Initialize the output of the model $\mathbf{G}^0(\mathbf{V}_p) = (0, \ldots, 0)$; for $p = 1, \ldots, P$. All along this algorithm, $\mathbf{G}^n(\mathbf{V}p) = [g_1^n(\mathbf{V}p), \ldots, g_M^n(\mathbf{V}p)]$ denotes the output of the network after locating the nth neuron.
2. Initialize the learning parameters for the variances and the centers, η_S and η_C, respectively; the final number of neurons N, and the standard deviation of the GRBF units according to the input data spread.
3. For $n = 1$ to N,
   3.1. Obtain the output error for the given model and the training data set:

$$E = \sum_p \sum_k \left(y_k(\mathbf{V}_p) - g_k^{n-1}(\mathbf{V}_p) \right)^2; \quad k = 1, \ldots, M \quad \text{and} \quad p = 1, \ldots, P. \quad (10)$$

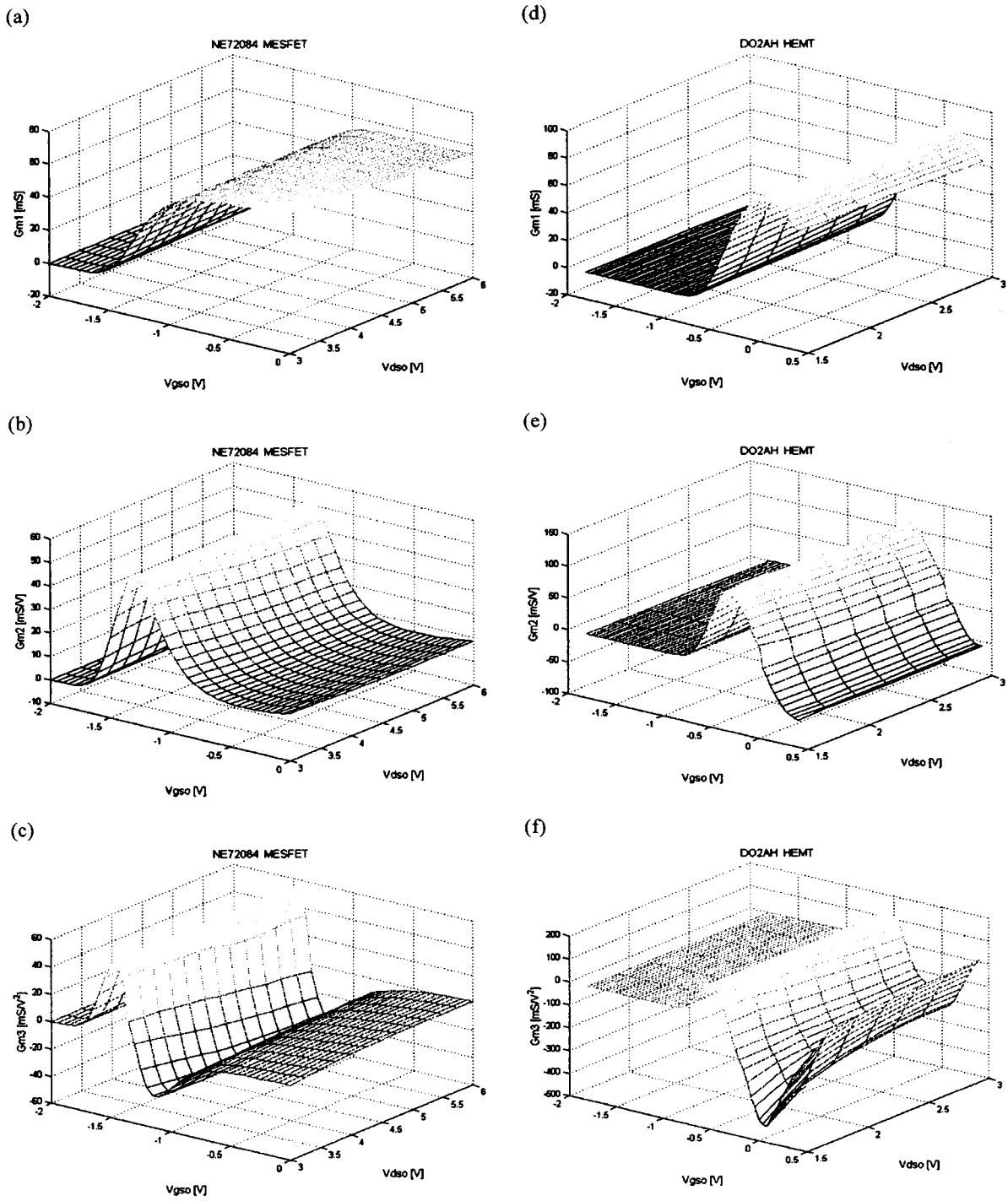

Figure 5. Experimentally extracted surfaces. Gm1 (a), Gm2 (b), and Gm3 (c) for a NE72084. Gm1 (d), Gm2 (e), and Gm3 (f) for a DO2AH.

3.2. Locate the new (nth) GRBF unit to get a maximum decrease in the error and assuming a fixed value for its variance. As the number of input data patterns is small, an exhaustive search for the center can be applied.

3.3. Update all the variances and centers by applying a gradient descent algorithm:

$$\sigma_{ij}^{k+1)} = \sigma_{ij}^{k)} - \eta_s \cdot \frac{\partial E}{\partial \sigma_{ij}}, \qquad i = 1, \ldots, n, \tag{11}$$

$$\mu_{ij}^{k+1)} = \mu_{ij}^{k)} - \eta_c \cdot \frac{\partial E}{\partial \mu_{ij}}, \qquad i = 1, \ldots, n, \tag{12}$$

where the gradients are given by (7) and (8), respectively.

The iterations are carried out until either the error decreases below a threshold value, or a maximum number of iterations is reached.

3.4. Estimate the amplitudes of the global GRBF network by solving the following linear least squares problem,

$$\begin{pmatrix} o_1(\mathbf{V}_1) \cdots o_n(\mathbf{V}_1) \\ \vdots \ \ddots \ \vdots \\ o_1(\mathbf{V}_P) \cdots o_n(\mathbf{V}_P) \end{pmatrix} \cdot \begin{pmatrix} \lambda_{11} \cdots \lambda_{M1} \\ \vdots \ \ddots \ \vdots \\ \lambda_{1n} \cdots \lambda_{Mn} \end{pmatrix} = \begin{pmatrix} y_1(\mathbf{V}_1) \cdots y_M(\mathbf{V}_1) \\ \vdots \ \ddots \ \vdots \\ y_1(\mathbf{V}_P) \cdots y_M(\mathbf{V}_P) \end{pmatrix}, \tag{13}$$

where $oi(\mathbf{V}p)$ is the output of unit i for pattern p, $Y_i(\mathbf{V}p) = [y_1(\mathbf{V}p), \ldots, yM(\mathbf{V}p)]$ is the pth target output, and λ_{ki} is the amplitude connecting the ith GRBF unit in the hidden layer to the kth unit in the output layer.

3.5. Obtain the new output of the GRBF network for the input patterns, $\mathbf{G}^n(\mathbf{V}_p)$, for $p = 1, \ldots, P$.

End.

IV. MESFETS AND HEMTS MODELING RESULTS

The experimentally extracted Taylor-series coefficients and the Ids DC value for a NE72084 MESFET and a DO2AH HEMT in their saturated regions were employed to train the proposed GRBF network in order to accurately model the Ids(Vgs, Vds) nonlinearity for small-signal IMD prediction. For the MESFET, Vdso was swept from 3 to 6 V in steps of 0.25 V and Vgso from −2V to 0 V with smaller steps of 0.05 V due to the stronger nonlinear dependence of all the outputs with this bias voltage, resulting in a total of 533 input–output training patterns. In the case of the HEMT, we varied Vdso between 1.5 and 3 V with 0.25 V steps, and Vgso between −1.8 and 0.4 V with 0.04 V steps obeying to the same reasons, here for a total of 392 patterns.

Three different neural network models were constructed: the highly local RBF network, the global MLP, and our GRBF network; in order to evaluate their accuracy and their cost (basically the number of parameters because the training set was the same) for this particular problem. We employed just one hidden layer; for N neurons in this layer, and taking into account we want to map **G**: $R^2 \rightarrow R^{10}$, a GRBF function and an MLP require $14N$ parameters, while $13N$ an RBF. The initial variance for the GRBF was selected according to the distance between the input patterns, $\sigma_i^2 = (0.025, 0.1)$ for the MESFET and $\sigma_i^2 = (0.05, 0.2)$ for the HEMT.

For evaluating the accuracy of each model, a "signal to noise ratio (SNR)" was employed as a figure of merit for each scalar output. Taking the predominant third order term, Gm3, as an example, its SNR would be defined as

$$\mathrm{SNR} = 10 \log_{10} \left(\frac{\Sigma_p G_{m3,p}^2}{\Sigma_p \left(G_{m3,p} - \hat{G}_{m3,p} \right)^2} \right), \tag{14}$$

where p indexes the training patterns, $G_{m3,p}^2$ is the desired output, and $\hat{G}_{m3,p}^2$ is the output the network estimates.

In Figures 6–8 we represent the MESFET and HEMT transconductance derivatives surfaces as obtained at the network outputs for an RBF with $N = 10$, an MLP and the proposed GRBF both with $N = 8$. The higher number of neurons in the

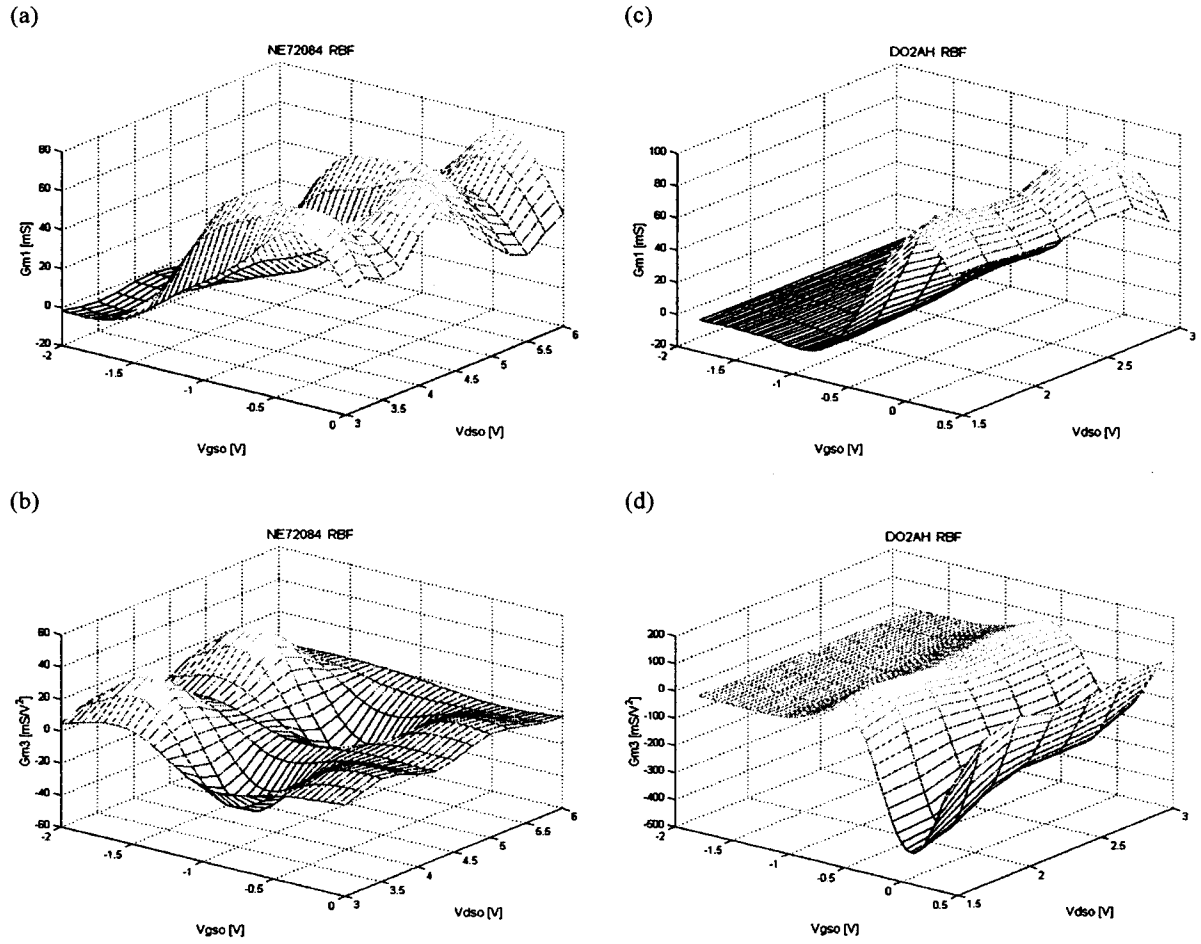

Figure 6. RBF network modeled surfaces. Gm1 (a) and Gm3 (b) for a NE72084. Gm1 (c) and Gm3 (d) for a DO2AH.

RBF network responds to the fact we want to compare accuracy for a similar number of parameters. These surfaces can be qualitatively compared to the respective measured ones, previously shown in Figure 5. While the MLP and GRBF models, of a more global nature, seem to capture the nonlinear behavior of these parameters, the highly local nature of the RBF solution determines excessively hilly output functions.

In Tables I and II we provide a more detailed quantitative comparison. First of all, it is significant that the GRBF network provides the best results for a small number of model parameters, and consequently a reduced cost. Second, taking into account the differences in SNR, achieving a similar performance would only be possible with an MLP of nearly twice as many parameters as the GRBF, and with an even higher amount for the RBF in the MESFET. These differences are not so marked in the HEMT where even the first order parameters, Gm1 and Gds have a strong nonlinear dependence with Vgso.

V. INTERMODULATION DISTORTION PREDICTION VALIDATION

The accuracy of this approach was only justified by the critical behavior of the C/I ratio in small-signal regime with both the bias voltages and the load condition in these devices. We are then forced to validate it with measurements and calculations of this linearity figure of merit for typical class A amplifiers applications.

For the bias dependence, we will show the predicted C/I behavior vs. Vgso at Vdso = 5 V in the saturated region of the characterized NE72084 MESFET, and at Vdso = 3 V for the

DO2AH HEMT in the same region. A standard two-tone excitation experiment was carried out with input frequencies of 2 and 2.01 GHz and 50 Ω load condition for an input power level per tone of −20 dBm well below the 1 dB compression point where Volterra calculations are valid. In Figure 9 we present the evolution of both the output power (Pout) and the C/I ratio vs. Vgso, making use of the experimental derivatives description and the GRBF network for both devices. We should remark about the good agreement in the results, as well as the reproduction of the optimum C/I point (sweet-spot) for the MESFET in its high gain region. Some differences appear in the pinch-off region where the derivatives have smaller values and the relative errors are greater, this bias region is however of low interest for the application of our concern.

On the other hand, simulations of load-pull IMD behavior in Figure 10 for the MESFET confirm previously published results [5, 23] about the existence of optimum load values for high C/I and high Pout trade-offs in highly linear designs. We employed a two-tone excitation at 10 and 10.01 GHz well in the microwave region trying to assure unconditional stability. As the Cgs(Vgs) contribution could be important at these frequencies, we employed its measured second and third order derivatives at this particular bias point, Vgso = −0.5 V and Vdso = 5 V.

The excellent load-pull description supports a precise reproduction not only of the predominant transconductance derivatives, but also of the cross terms responsible for this peculiar C/I behavior. This feature is hardly obtained with most of the analytical models, validating a neural network

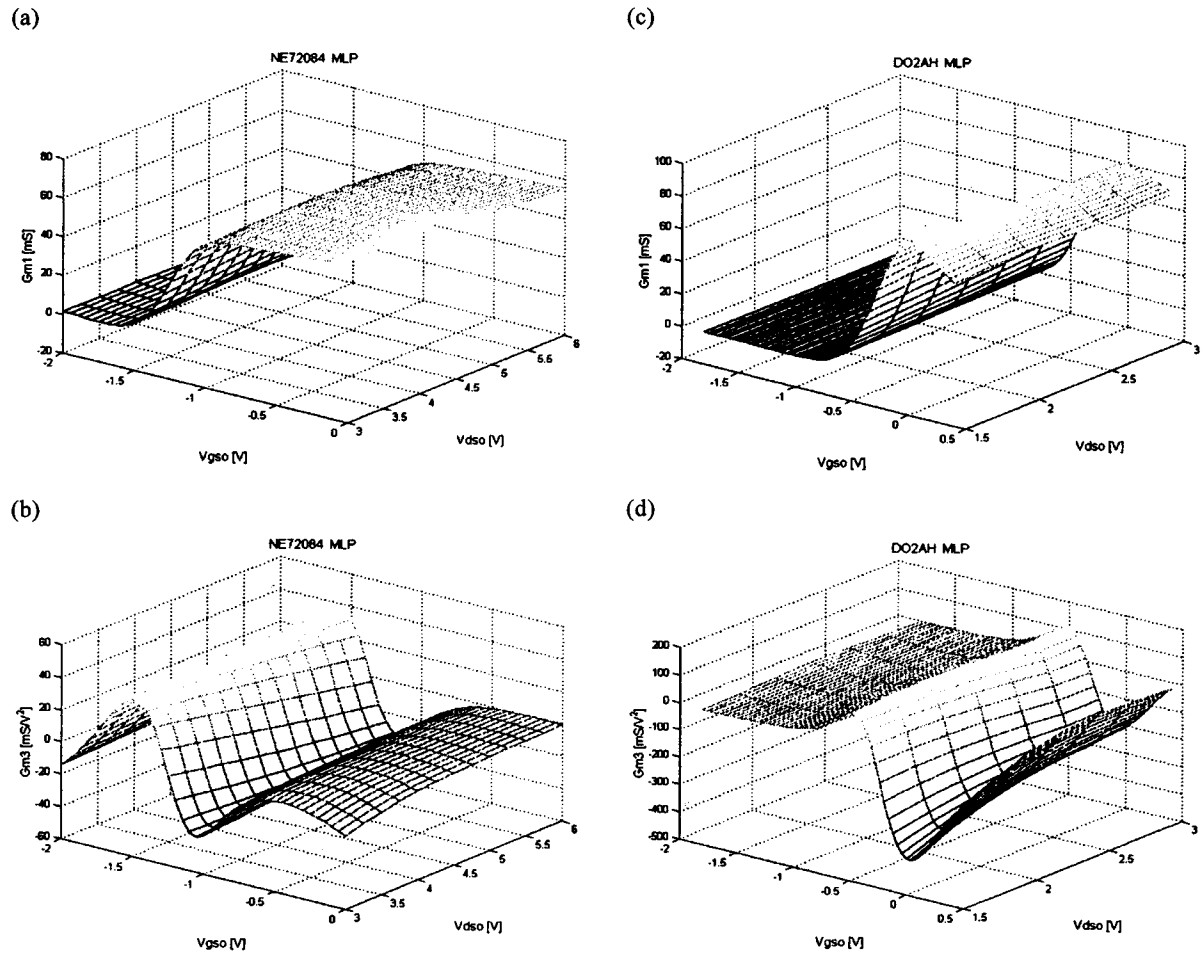

Figure 7. MLP network modeled surfaces. Gm1 (a) and Gm3 (b) for a NE72084. Gm1 (c) and Gm3 (d) for a DO2AH.

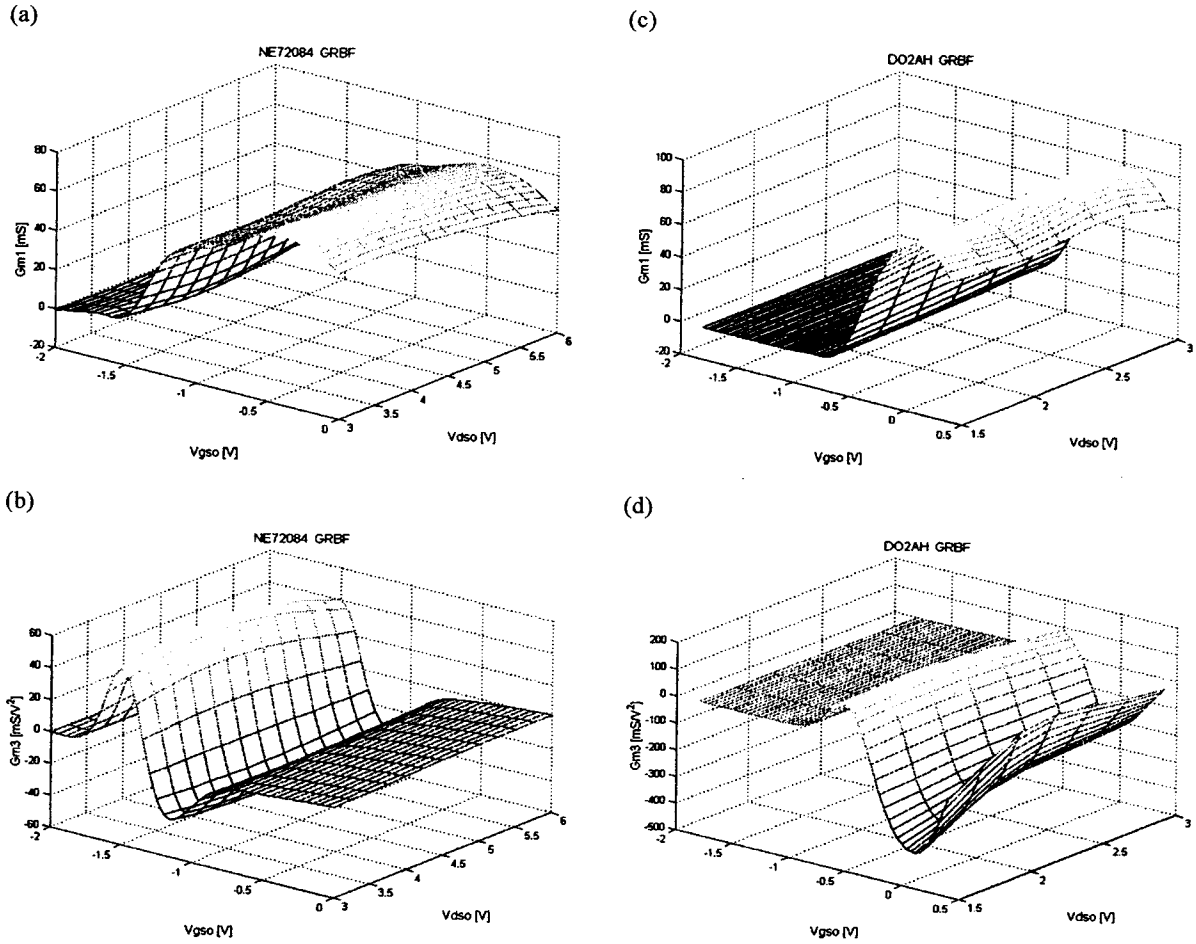

Figure 8. GRBF network modeled surfaces. Gm1 (a) and Gm3 (b) for a NE72084. Gm1 (c) and Gm3 (d) for a DO2AH.

TABLE I. Comparison of Neural Networks Modeling Results for a NE 72084 MESFET: GRBF ($N = 8$), RBF (10), and MLP (8)[a]

	Npar	Ids	Gm1	Gds	Gm2	Gmd	Gd2	Gm3	Gm2d	Gmd2	Gd3
GRBF (8)	112	22.8	27.2	25.4	17.0	17.9	19.1	18.5	18	16.09	15.7
RBF (10)	130	12.0	12.0	12.3	6.4	6.3	10.7	2.3	3.5	3.6	9.5
MLP (8)	112	20.0	30.0	24.6	13.5	13.6	13.5	8.9	9.9	10.7	14.0

[a]The first column indicates the number of parameters for each model, the following 10 columns show the SNR in dB for each output of the model.

TABLE II. Comparison of Neural Networks Modeling Results for a DO2AH HEMT: GRBF ($N = 8$), RBF (10), and MLP (8)[a]

	Npar	Ids	Gm1	Gds	Gm2	Gmd	Gd2	Gm3	Gm2d	Gmd2	Gd3
GRBF (8)	112	24.3	29.8	28.7	24.1	26.2	21.5	17.5	16.0	16.7	10.8
RBF (10)	130	18.4	19.8	20.7	14.6	13.9	19.8	14.5	13.9	14.8	15.0
MLP (8)	112	24.7	30.5	27.4	19.8	24.6	21.1	16.2	14.1	13.0	13.1

[a]The first column indicates the number of parameters for each model, the following 10 columns show the SNR in dB for each output of the model.

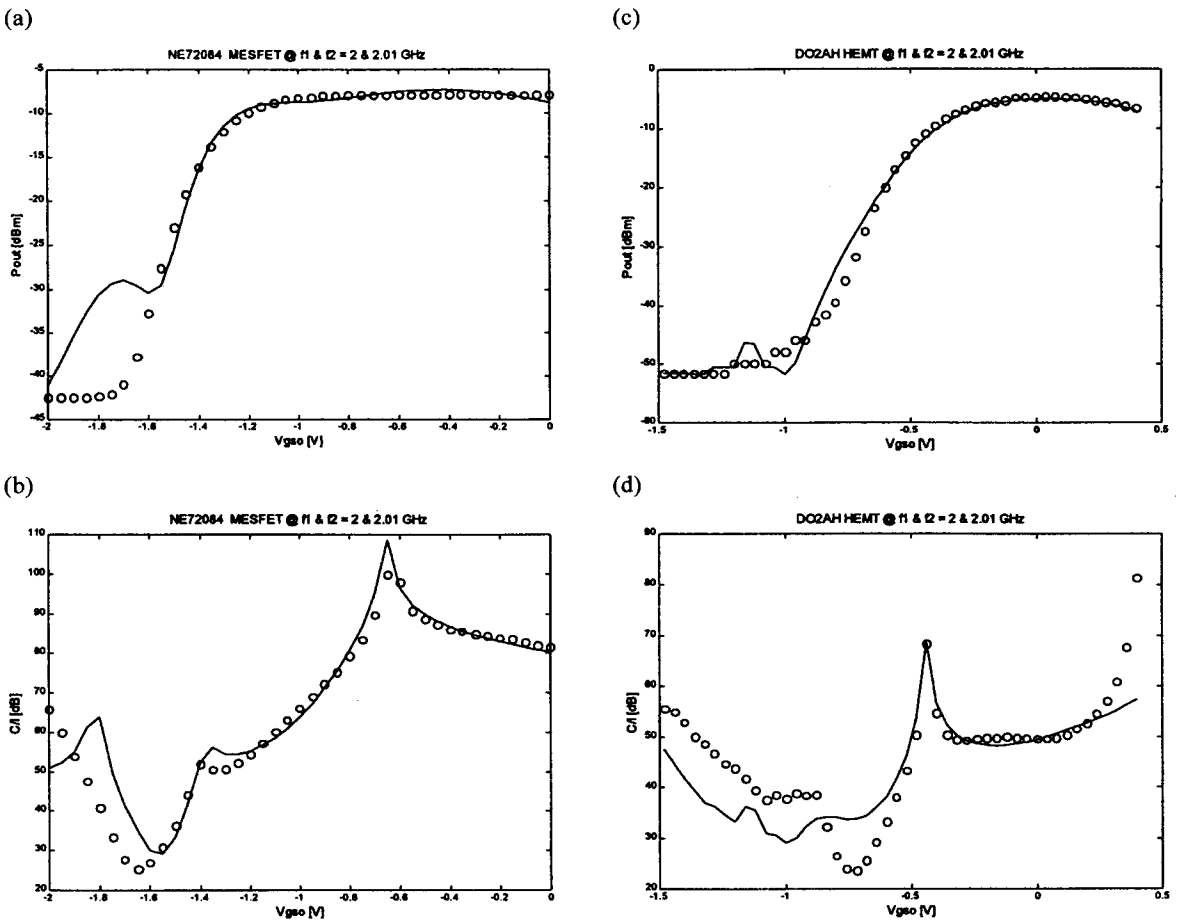

Figure 9. Two-tones excitation Pout (@f1 = 2GHz) and C/I (@2f1 − f2 = 1.99 GHz) vs. gate to source bias. Pout (a) and C/I (b) for a NE72084. Pout (c) and C/I (d) for a DO2AH. (open circles) With the experimental coefficients, (solid line) GRBF network model.

approach when such an accurate IMD control is needed.

VI. CONCLUSIONS

A neural network model for the nonlinearity Ids(Vgs, Vds), that basically determines the IMD behavior of MESFETs and HEMTs in their saturated region, has been presented for an accurate description of this relevant nonlinear distortion. The proposed GRBF network allows different variances for each dimension of the input space, thus taking advantage of the soft nonlinear dependence of the Taylor-series coefficients with the drain to source bias voltage (a sort of knowledge-based neural network). This results in a parsimonious and accurate model adequate for small-signal IMD calculations with a Volterra-series simulator.

Our GRBF network requires a reduced number of parameters when compared to the RBF and MLP networks for this particular problem. The agreement in C/I prediction with bias and load supports its robust performance for the small-signal quasilinear description of this nonlinearity.

The Cgs(Vgs) minor nonlinearity power-series expansion could be also described by this technique using a similar procedure. Linear region description where the coefficients are strongly dependent of both bias voltages could be incorporated with an analogous approach and a region description as the one proposed in [15].

ACKNOWLEDGMENT

This work has been partially supported by CYCIT Grant TIC996-0500-C10-07.

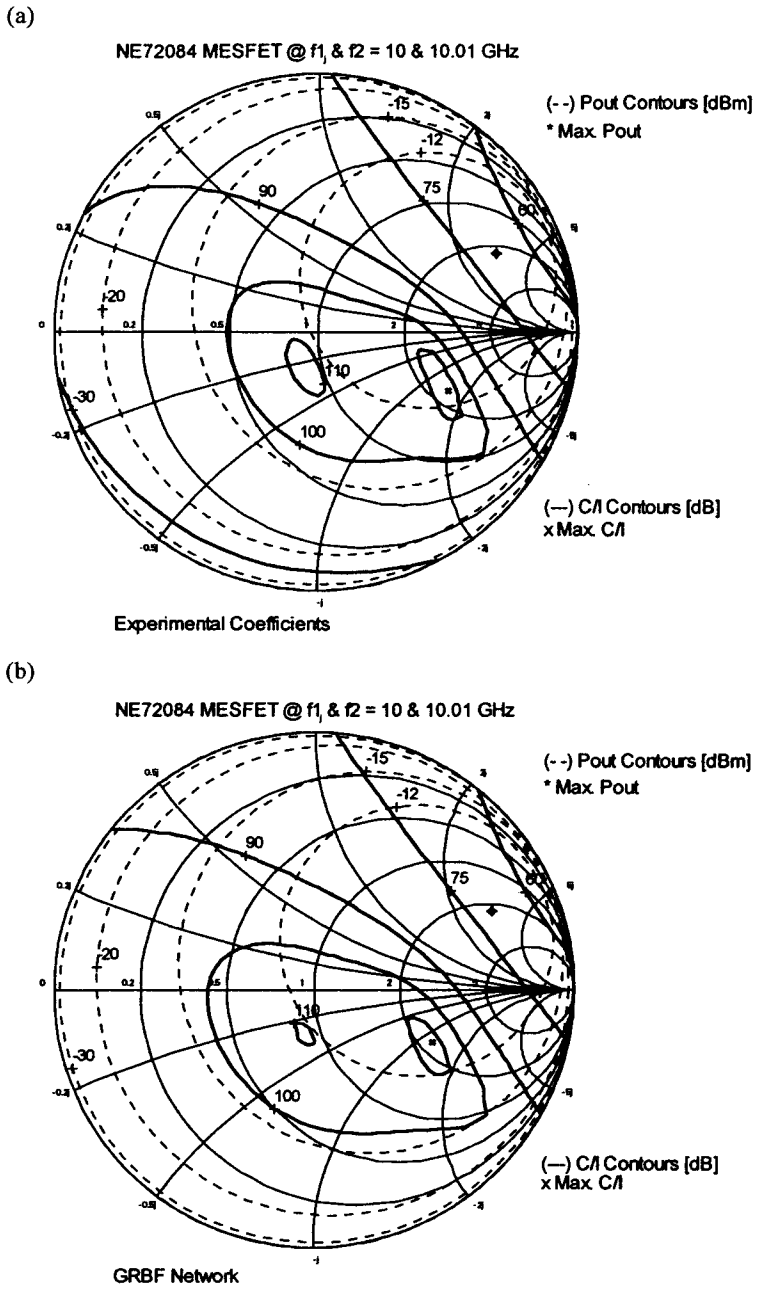

Figure 10. C/I and output power load-pull contours: (a) With the experimental coefficients, (b) GRBF network model.

REFERENCES

1. J.M. Golio, Microwave MESFETs and HEMTs, Artech House, Norwood, MA, 1991.
2. R. Anholt, Electrical and thermal characterization of MESFETs, HEMTs and HBTs, Artech House, Norwood, MA, 1995.
3. S. Maas, How to model intermodulation distortion, IEEE MTT-S International Microwave Symposium Digest, 1991, pp. 149–151.
4. S.A. Maas and D. Neilson, Modeling MESFETs for intermodulation analysis of mixers and amplifiers, IEEE Trans Microwave Theory Tech 38 (1990), 1964–1971.
5. J. Pedro and J. Perez, Accurate simulation of GaAs MESFETs intermodulation distortion using a new drain-source current model, IEEE Trans Microwave Theory Tech 42 (1994), 25–33.
6. J.A. García, A. Mediavilla, J.C. Pedro, N.B. Carvalho, A. Tazón, J.L. García, Characterizing the

gate to source nonlinear capacitor role on FET IMD performance," IEEE MTT-S International Microwave Symposium Digest, 1998, pp. 1635–1638.
7. P.B.L. Meijer, Fast and smooth highly nonlinear multidimensional table models for device modeling, IEEE Trans Circuits Syst 37 (1990), 335–346.
8. P.M. Watson and K.C. Gupta, EM-ANN models for microstrip vias and interconnects in dataset circuits, IEEE Trans Microwave Theory Tech 44 (1996), 2495–2503.
9. A. Veluswami, M.S. Nakhla, and Q.J. Zhang, The application of neural networks to EM-based simulation and optimization of interconnects in high speed VLSI circuits, IEEE Trans Microwave Theory Tech 45 (1997), 712–723.
10. G.L. Creech, B.J. Paul, C.D. Lesniak, T.J. Jenkins, and M. Calcatera, Artificial neural networks for fast and accurate EM-CAD of microwave circuits, IEEE Trans Microwave Theory Tech 45 (1997), 794–802.
11. P.M. Watson and K.C. Gupta, Design and optimization of CPW circuits using EM-ANN models for CPW components, IEEE Trans Microwave Theory Tech 45 (1997), 2515–2523.
12. P. Burrascano, M. Dionigi, C. Fancelli, and M. Mongiardo, A neural network model for CAD and optimization of microwave filters, IEEE MTT-S International Microwave Symposium Digest, 1998, pp. 13–16.
13. A.H. Zaabab, Q. Zhang, and M. Nakhla, A neural network modeling approach to circuit optimization and statistical design, IEEE Trans Microwave Theory Tech 43 (1995), 1349–1358.
14. A.H. Zaabab, Q. Zhang, and M. Nakhla, Device and circuit-level modeling using neural networks with faster training based on network sparsity, IEEE Trans Microwave Theory Tech 45 1696–1704, (1997).
15. F. Wang and Q. Zhang, Knowledge-based neural models for microwave design, IEEE Trans Microwave Theory Tech 45 (1997), 2333–2343.
16. K. Shirakawa, M. Shimiz, N. Okubo, and Y. Daido, A large-signal characterization of an HEMT using a multilayered neural network, IEEE Trans Microwave Theory Tech 45 (1997), 1630–1633.
17. J. Rousset, Y. Harkouss, J.M. Collantes, and M. Campovecchio, An accurate neural network model of FET intermodulation and power analysis, 26th Europ Microwave Conf Proceedings, 1996, pp. 16–19.
18. P.M. Watson, K.C. Gupta, and R.L. Mahajan, Development of knowledge based artificial neural networks for microwave components, IEEE MTT-S International Microwave Symposium Digest, 1998, pp. 9–12.
19. J.J. Bussgang, L. Ehrman, and J.W. Graham, Analysis of nonlinear systems with multiple inputs, Proc IEEE, 62 (1974), pp. 1088–1119.
20. S.A. Maas, Nonlinear microwave circuits, Artech House, Butler, WI, 1988.
21. A. Mediavilla, A. Tazón, J.L. García, T. Fernández, J.A. García, J.M. García, C. Navarro, and J.M. Zamanillo, Dynamic properties and modeling of large signal, thermal, optical, and intermodulation effects in microwave GaAs devices, WMC Nonlinear Measuring and Modeling Workshop, IEEE MTT-S International Microwave Symposium, 1997.
22. G. Dambrine, A. Cappy, F. Heliodore, and E. Playez, A new method for determining the FET small-signal equivalent circuit, IEEE Trans Microwave Theory Tech 36 (1988), 1151–1159.
23. D.R. Webster, D.G. Haigh, G. Passiopoulos, and A.E. Parker, Distortion in short channel FET circuits, Low-power HF microelectronics, G. Machado, (Editor), IEE, London, U.K., 1996, pp. 929–958.
24. S. Haykin, Neural networks: a comprehensive foundation, Macmillan Co., New York, 1994.
25. T. Poggio and F. Girosi, Networks for approximation and learning, Proc IEEE, 78 (1990), pp. 1481–1497.
26. E. Hartman and J.D. Keeler, Predicting the future: advantages of semilocal units, Neural Comput 3 (1991), 566–578.

BIOGRAPHIES

José Angel García was born in Havana, Cuba, in 1966. He graduated (with honors) in telecommunications engineering from the "José A. Echeverría" Institute of Technology (I.S.P.J.A.E.) in 1988. From 1988 to 1991 he was a radio system engineer at an HF Communication Center. In 1991, he was appointed instructor professor at I.S.P.J.A.E. Since 1995, he has been a Ph.D. student at the University of Cantabria, Spain, with a MUTIS grant. His main research interests include nonlinear characterization and modeling of active devices as well as nonlinear circuits analysis tools for amplifiers and mixers applications. IEEE Student Member (1998).

Antonio Tazón Puente was born in Santander, Spain, in 1951. He graduated in 1978 and received the Doctor of Physics degree in 1987, both from the University of Cantabria, Santander, Spain. From 1991 to 1995 he was a professor at the Department of Electronics University of Cantabria and since 1996 he has been a professor at the Department of Commu-

nication Engineering also of the University of Cantabria, Spain. In 1985, from March to October and in 1986, from April to July, he carried out stages at the IRCOM Department (University of Limoges, France) working in nonlinear modeling and load-pull techniques. He has participated in Spanish and European projects in the nonlinear modeling (Esprit project 6050 MANPOWER) and microwave and millimeter wave communication circuits and systems (Spanish Project PlanSAT, European Project CABSINET, etc). He has carried out research on analysis and optimization of nonlinear microwave active devices and circuits in both hybrid and monolithic technologies. Currently his main research interests are the active microwave circuits, mainly in the area of linear and large-signal modeling and small signal intermodulation of GaAs and Si-Ge devices and their applications in nonlinear computer design. IEEE Member (1992).

Angel Mediavilla Sánchez was born in Santander, Spain, in 1955. He graduated (with honors) in 1978 and received the Doctor of Physics degree in 1984, both from the University of Cantabria, Santander, Spain. From 1980 to 1983 he was Ingénieur Stagière at Thomson-CSF, Corbeville, France. Now, he is a professor at the Department of Electronics of the University of Cantabria. He has a wide experience in analysis and optimization of nonlinear microwave active devices and circuits in both hybrid and monolithic technologies. He has participated in Spanish and European projects in nonlinear modeling (Esprit project 6050 MANPOWER) and microwave and millimeter wave communication circuits and systems (Spanish Project PlanSAT, European Project CABSINET, etc). His current research fields are on active microwave circuits, mainly in the area of nonlinear modeling of GaAs devices and their applications in large-signal computer design. IEEE Member (1992).

Ignacio Santmaría was born in Vitoria, Spain, in 1967. He received the Telecommunication Engineer degree and the Doctor degree from the Universidad Politécnica de Madrid (UPM), Spain, in 1991 and 1995, respectively. In 1992 he joined the Departamento de Ingeniería de Comunicaciones at the Universidad de Cantabria, Spain, where he is currently an associate professor. His research interests include digital signal processing, nonlinear systems, and neural networks. IEEE Member (1996).

Marcelino Lázaro was born in Carriazo, Spain, in 1972. He received the Telecommunications Engineer degree from the Universidad de Cantabria, Spain, in 1996. Currently he is working at the Departamento de Ingeniería de Comunicaciones of the Universidad de Cantabria as a postgraduate student. His research interests include digital signal processing, nonlinear modeling, and neural networks.

Carlos J. Pantaleón was born in Badajoz, Spain, in 1966. He received the Telecommunication Engineer degree and the Doctor degree from the Universidad Politécnica de Madrid (UPM), Spain, in 1990 and 1994, respectively. In 1990 he joined the Departamento de Ingeniería de Comunicaciones at the Universidad de Cantabria, Spain, where he is currently an associate professor. His research interests include digital signal processing, nonlinear systems, and neural networks. IEEE Member (1996).

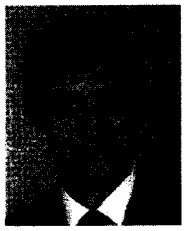

José Carlos Pedro was born in Espinho, Portugal on March 7, 1962. He received the diploma and doctoral degrees in electronics and telecommunications engineering, from University of Aveiro, Portugal, in 1985 and 1993, respectively. From 1985 to 1993 he was an assistant lecturer at the University of Aveiro, and a professor since 1993. Currently he is an associate professor at the same university, and a senior research scientist at the Telecommunications Institute. His main scientific interests include active device modeling and the analysis and design of various nonlinear microwave and optoelectronics circuits, in particular, the design of highly linear multicarrier power amplifiers. Dr. Pedro received the Marconi Young Scientist Award in 1993. IEEE Student Member (1990), IEEE Member (1995).